

AD-A106 328

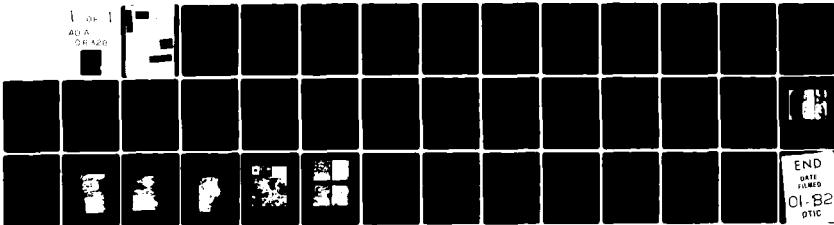
ATOMIC ENERGY RESEARCH ESTABLISHMENT HARWELL (ENGLAND) F/6 11/6
THE OXIDATION OF DILUTE IRON-SILICON ALLOYS ((SI) < OR = 1 W/O)--ETC(U)
FEB 81 P T MOSELEY, G TAPPIN, J C RIVIERE

UNCLASSIFIED

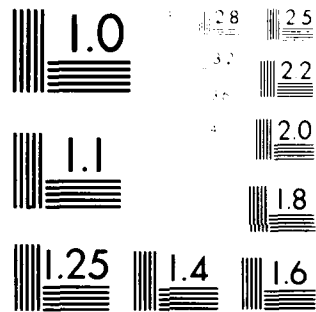
AERE-R-10042

NL

1 of 1
AD A
DA 128



END
DATE
FILMED
01-82
DTIC



MICROCOPY RESOLUTION TEST CHART
NBS 1963-A

AD 11 088328

LEVEL

DTIC
DEC 1 1981

DATE RECORDED
1981

The Oxidation of Dilute Iron-Silicon Alloys
([Si] \leq 1^{w/o}) in Carbon Dioxide

P.T. Moseley, G. Tappin, and J.C. Rivière

Abstract

The manner in which silicon, present as a minor alloy constituent, modifies the oxidation of iron in CO₂/1% CO at 500°C has been studied. Increasing amounts of silicon progressively reduce the oxidation rate within the range [Si] = 0-1^{w/o} and a variety of physical techniques have been used to examine oxidized specimens in pursuit of the origins of this beneficial influence. The scale forming on the alloys is composed of two layers in each of which iron is present as Fe₃O₄. The inner layer of scale contains silicon at approximately the same level (on a volume % basis) as the original metal while the outer scale appears to contain no silicon. The boundary between the two layers is also marked by an abrupt change in grain size and in texture of the Fe₃O₄.

At the boundary between the alloy and the scale there develops a thin layer of non-ferrous material in which the concentration of silicon is increased by more than an order of magnitude above that in the bulk alloy. This layer also includes a substantial accumulation of carbon which is thought to derive from carbon oxide gases which have penetrated to the base of the scale before taking part in the oxidation reaction.

The observation of the layer of non-ferrous material between the alloy and the scale constitutes a qualitative agreement with theoretical studies which indicate that the reduction in oxidation rate conferred by the presence of silicon in the alloy is at least partly due to the impeded passage of Fe³⁺ ions from the alloy into the scale.

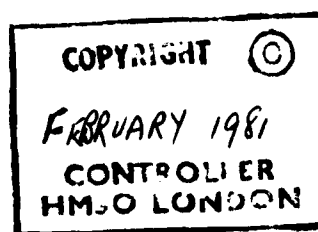
Materials Development Division,
AERE Harwell.

February 1981

HL 81/515 (C14)

DISTRICT

Approved for public release
Distribution Unlimited



Contents

	<u>Page No.</u>
1. Introduction	1
2. Experimental and Results	2
2.1 Specimens and Oxidation Conditions	2
2.2 X-Ray Diffraction: Texture of Scales	2
2.3 Kinetics	4
2.4 Electron Microscopy	4
2.5 X-Ray Photoelectron Spectroscopy (XPS)	6
2.6 Mössbauer Spectroscopy	9
3. Discussion	9
Acknowledgements	11
References	12

Accession No. _____

NTIS GRA&I _____

DTIC TAB _____

Unannounced _____

Justification _____

By _____

Distribution _____

Availability _____

Dist _____

A

Tables

1. Silicon content of iron-silicon alloys, wt. %.
2. Texture coefficients $T_{h'k'l'}$ of alloys and scales.
3. Mean kinetic constants (and standard deviation) for iron and iron-silicon alloys oxidized in CO_2 1% CO at 500°C .
4. Wavelength dispersive X-ray analysis of polished sections through scales on 5 specimens.
5. The energy separation (in eV) of the Si 2p and O1s peaks for oxygen-containing silicon compound standards after $50 \mu\text{A min}$ ion bombardment at 5 keV.
6. The energy separation (in eV) of the Si 2p and O1s peaks for scales on the alloys Fe/0.4^w/o Si and Fe/1.0^w/o Si as a function of ion bombardment dose (experimental error ± 0.1 eV)

Figures

1. X-ray powder diffraction patterns. A. Outer surface of scale grown on α iron in $\text{CO}_2/900$ vpm air. B. Standard random pattern of α Fe_2O_3 .
2. X-ray powder diffraction patterns. A. Outer surface of scale grown on α iron in $\text{CO}_2/1\%$ CO . B. Standard random pattern of Fe_3O_4 .
3. Weight gain curves of pure iron and iron silicon alloys oxidized in $\text{CO}_2/1\%$ CO at 500°C .
4. Scanning electron micrograph of section through metal and scale on Fe 1^w/o Si. The trace is a scan for silicon made along the indicated line. Note that the zero of silicon signal is not on this line, but corresponds to the value in the outer part of the scale.
5. (a) Development of oxide scale on a metal surface and preparation of (b) parallel and (c) transverse specimens for electron microscopy.
6. Transverse transmission electron micrographs of scale grown on a specimen of Fe 0.1^w/o Si. (a) Outer scale, (b) Boundary between outer and inner scale (arrowed) and (c) Boundary between inner scale and metal.
7. Plan transmission electron micrograph of material taken from between the metal and the oxide scale after oxidation of an Fe 1^w/o Si alloy in $\text{CO}_2/1\%$ CO at 500°C for 3 months. Insets show an EDAX spectrum and a diffraction pattern from this material.
8. SEM image (a) together with oxygen (b), silicon (c) and carbon (d) maps (all x 800) of material from between Fe 1^w/o Si and scale.

9. Depth profile of elemental composition measured by XPS. The initial surface at zero ion dose was that of the underside of the scale grown on pure Fe. Erosion by an ion beam coupled with XPS analysis then gave the composition as a function of distance into the oxide.
10. Depth profile of elemental composition measured by XPS. The initial surface at zero ion dose was that of the underside of the scale grown on the Fe/0.1^w/o Si alloy. Erosion by an ion beam coupled with XPS analysis then gave the composition as a function of distance into the oxide.
11. Depth profile of elemental composition measured by XPS. The initial surface at zero ion dose was that of the underside of the scale grown on the Fe/0.4^w/o Si alloy. Erosion by an ion beam coupled with XPS analysis then gave the composition as a function of distance into the oxide.
12. Depth profile of elemental composition measured by XPS. The initial surface of zero ion dose was that of the underside of the scale grown on the Fe/1^w/o Si alloy. Erosion by an ion beam coupled with XPS analysis then gave the composition as a function of distance into the oxide.
13. Variation of maximum peak silicon concentration in the interfacial layer as a function of silicon concentration in the alloy.
14. Schematic drawing of near-surface region of Fe/Si alloy before and after protective oxidation with qualitative indication of silicon distribution.
15. Variation of apparent parabolic rate constant for oxidation of Fe/Si alloys plotted as a function of silicon content.

1. INTRODUCTION

The scaling resistance of a number of high temperature ferrous alloys [1,2] is significantly enhanced by the presence of silicon. This element offers the twin benefits that it is effective at levels sufficiently low not to affect mechanical properties of the alloys significantly and that it is plentiful. Silicon generally finds applications in conjunction with a number of other alloying elements, but it has been reported [3] that even in the binary alloy it brings a substantial reduction in the rate of oxidation in an oxygen pressure of 0.2 atm; the addition of silicon to iron (up to 5.3^{w/o} Si) reduced the oxidation rate at all temperatures between 500 and 1000°C and an enrichment of silicon was detected by the electron microprobe near the metal/oxide phase boundary. The oxidation rate of copper-silicon alloys also falls with increasing silicon content. Recently it has been shown [4] that the oxidation rate ($P_{O_2} = 0.01$ atm, 800-1000°C) of copper-silicon alloys containing up to 4.5^{w/o} silicon was reduced with respect to pure copper by the formation of amorphous flakes of SiO₂ at the alloy/scale interface and, at the maximum alloy silicon content, by a continuous layer of SiO₂. During studies of the scale formed on iron-chromium-silicon alloys containing up to 5.1^{w/o} silicon a complete SiO₂ layer was revealed between the Cr₂O₃ scale and the alloy [5]. The detection of silicon near the alloy/scale interface represents a common factor amongst these various systems.

The aim of the present work is to carry further the study of the effect of low levels of silicon in iron-silicon alloys on the composition of the oxide scale and on the kinetics and mechanism of scale formation. In view of the acknowledged importance of low levels of silicon ($\sim 0.6^w/o$) in various steels for nuclear applications [6] the work takes the form of an isothermal study at 500°C of the oxidation of iron-silicon alloys in the range Si = 0-1^{w/o} in CO₂ containing 1^{v/o} CO.

2. EXPERIMENTAL AND RESULTS

2.1 Specimens and Oxidation Conditions

Samples of polycrystalline iron doped with nominal amounts of 0, 0.1, 0.3 and 0.7^{w/o} of silicon were supplied by Metals Research Ltd. The actual compositions of the samples used here, as analysed by X-ray fluorescence, are given in Table 1. Coupons of each composition were rolled to a thickness of ~ 1 mm, cut to size 10 x 15 mm, degreased, annealed for 2 hours in argon at 900°C and polished to a 1 micron diamond finish. The coupons were suspended in a horizontal tube furnace in a stream of dried (magnesium perchlorate) carbon dioxide at atmospheric pressure and 500°C. Initially the gas stream contained 900 vpm of air and the scales developed an outermost layer of Fe₂O₃. The gas was switched to 99% CO₂/1% CO for the remainder of the programme and Fe₃O₄ became the sole iron oxide among the reaction products as expected.

2.2 X-Ray Diffraction: Texture of Scales

Specimens were examined with the aid of a powder diffractometer and a texture goniometer attachment on the Harwell APEX system. The outer surface of the scale was examined in situ on the coupon and the inside of the scale was examined after removal of the alloy substrate in an iodine-methanol mixture.

As mentioned earlier the outside of the scale formed in the gas (CO₂ + 900 vpm air) used initially was contaminated with Fe₂O₃ and X-ray diffraction showed (Figure 1) that this oxide had a huge orientation preference - mainly for h00 (hexagonal) poles but with a minor population of hh0 (hexagonal) poles. By way of comparison we note that iron-silicon alloys oxidized in 0.2 atmospheres of oxygen [3] produced Fe₂O₃ with (110) orientation at 800°C and (001) orientation at 1000°C. Chromium steels oxidized in air at 500-700°C [7] yielded a rhombohedral scale which was reported to be heavily oriented with (111) (i.e. hexagonal (001)) planes parallel to the surface. Evidently both the temperature and the atmosphere of oxidation exert some influence on the preferred orientation adopted by the

scale. Fe_3O_4 scales developed during the rest of the programme showed modest preference for the cubic h00 texture (Figure 2). In none of the oxide scales (except possibly that formed on pure iron) was the texture attributable to initial texture in the alloy coupons.

The preferred orientation information is extracted from the diffraction patterns in the form of texture coefficients, $T(h'k'l')$, for the favoured reflections $h'k'l'$, and is given in Table 2.

$T(h'k'l')$ is defined as

$$\frac{I_{h'k'l'} / I_{h'k'l'}^0}{1/n \sum_0^n (I_{hkl} / I_{hkl}^0)}$$

where I_{hkl} refers to the measured intensity of reflection hkl , I_{hkl}^0 refers to the intensity of the same reflection from a randomly oriented specimen and n reflections are considered. $T(h'k'l')$ exceeds unity when $h'k'l'$ poles are oriented perpendicular to the reference surface more than in the random case [8].

X-ray diffraction patterns of the inside surface of all the scales showed these to be composed of Fe_3O_4 also but with a less pronounced texture than the outer scales. The lattice parameters at the inner and outer surface of the scale were typically 8.3966 (4) and 8.3964 (3) Å respectively which is an indication that any deviation from stoichiometry of the magnetite was very small [9,10].

In addition to the magnetite pattern the diffraction pattern from the inside surface of the scale on Fe 1^w/o Si specimens showed a very broad peak (1.5° at half height). This peak was centred at a point corresponding to an interplanar spacing of 3.4 Å and therefore might be ascribed to poorly crystalline silica or to graphite (SiO_2 $d_{101} = 3.34$ Å, graphite $d_{200} = 3.36$ Å).

The diffraction pattern from the inside surface of the scale on some, but not all, pure iron specimens included the pattern of cementite Fe_3C . When cementite was absent from the inside surface of

the scale on pure iron Fe_3O_4 was the only phase detected. Cementite is metastable with respect to iron and graphite and its inconsistency in formation may have been due to differences in cooling rate.

2.3 Kinetics

The kinetics of oxidation were followed by interrupting the furnace treatment to weigh the specimens at room temperature. A comparative plot of the progress of the protective stage of oxidation for samples of the four compositions (Figure 3) shows that the rate of oxidation falls with increasing silicon content. Kinetic data, averaged for several coupons of each composition are given in Table 3. In order that comparisons may be made with other data in the literature the rate constants have been calculated by a least squares fit with the parabolic rate equation. The parabolic rate constant for iron is below that measured for iron in CO_2 at 550°C [11] and decreases with increasing silicon content of the alloy. When, alternatively, the data are fitted to an equation of the form $\Delta w = kt^n$ it is found that the value of n (which would be 0.5 for parabolic kinetics) falls progressively with increasing silicon content.

2.4 Electron Microscopy

Scanning electron microscopy (SEM) of polished sections confirmed that the scales formed on the iron-silicon alloys were duplex and an elemental line scan (Figure 4) showed that silicon was present at a uniform level through the inner part, but was not significantly above background in the outer part of the scale. The volume fraction of silicon in the inner scale was in general only slightly greater than in the alloy. Quantitative analyses of metal and inner and outer scales in polished sections are given in Table 4. Measurements of silicon concentration on two specimens of 1W/o Si scale at different weight gains suggest that the amount of silicon in the inner scale is not increasing with oxidation.

Specimens were prepared for transmission electron microscopy by a range of techniques selected to provide as much microstructural

information as possible. Figure 5(a) shows schematically a section through metal and scale with oxidation in progress. For a proper investigation of the scale microstructure it was essential to be able to study both plan (Figure 5b) and transverse (Figure 5c) sections. Plan specimens were prepared by removing the alloy in an iodine methanol mixture and thinning with an ion beam mill (Iontech Microlap, 5 kV, argon) until they were transparent to electrons. By selectively etching from one side more than the other or from one side alone it was possible to prepare thin sections (a) from within the outer scale, (b) from within the inner scale and (c) from that part of the scale which had been adjacent to the metal. Transverse specimens were prepared by polishing sections of substrate-plus-oxide with diamond paste to a thickness of roughly 50 microns and then ion beam milling.

Transmission electron micrographs of transverse sections (Figure 6) showed that the grains of the outer scale on iron-silicon alloys tended to be elongated in the direction of growth (normal to the surface) and that the boundary between inner and outer scales is marked by an abrupt change in grain size (see Figure 6b). The boundary was quite straight in all sections where it was observed. There is incomplete contact between the scale and the metal surface (Figure 6c). Over a considerable fraction of the surface the oxide and the metal are separated by regions of porosity and/or precipitate phases.

Characteristic X-ray analysis of plan specimens in the transmission electron microscope (TEM) showed no trace of silicon in the outer scale on Fe 1^w/o Si, but considerable quantities of silicon distributed irregularly through the inner scale. These areas of high silicon content could not be identified with specific contrast features nor with a diffraction pattern. A plan specimen from scale adjacent to the metal revealed areas emitting X-rays almost entirely attributable to silicon. These areas too were not identifiable with visible features and yielded diffraction patterns characteristic of amorphous material.

It was evident that there was an accumulation of silicon in the vicinity of the metal-scale interface, so this silicon-rich layer was examined by separating it entirely from all ferrous material. This was done by first removing the metal alloy by dissolving in an iodine

methanol mixture, and then removing the ferrous oxides in a bath of dilute hydrochloric acid. The remnant layer was recovered on a microscope grid, and was transparent to electrons without further treatment. It emitted principally silicon X-rays with small contributions from chlorine and copper in some places. Bright field images of this layer (e.g. Figure 7) showed a fibrous structure with a good deal of free space in some parts and accumulations of material in other parts. The diffraction pattern from all parts of the specimen consisted of a very broad ring pattern with an initial spacing at 3.4-3.8 Å (Figure 7).

Pieces of the same specimen were examined in the Camebax electron probe microanalyser. High levels of silicon, carbon and oxygen were evident and these are displayed in map form together with the SEM image in Figure 8. Quantitative analysis of an area 40 µm x 10 µm yielded carbon 29.4%, silicon 10.2%, oxygen 12.1%, iron 0.8% (all by weight) and a substantial contribution from the copper support grid. The silicon and oxygen figures are in approximately the proportion to be expected for silica.

A layer similar in appearance to that shown in Figure 7 was recovered from an oxidized coupon of Fe 0.4^{w/o} Si and energy dispersive X-ray analysis indicated that this layer also included a substantial amount of silicon.

The layers are apparently composed of silica and carbon and for the dilute iron-silicon alloys examined they are probably no more than 1000-2000 Å thick so that they are not easily characterized by end-on observation. The SEM line scan in Figure 5 did not sense an enrichment of silicon because the probe diameter (1 µm) was considerably larger than the thickness of the silica-rich layer.

Further information was therefore sought using surface techniques on plan specimens.

2.5 X-Ray Photoelectron Spectroscopy (XPS)

Since the technique of XPS needs a large (several mm²) area for analysis, specimens for examination by XPS were prepared specially by

vapour-deposition of a relatively thick layer of platinum on the outside of the scale before stripping in iodine-methanol. In this way sufficiently large areas could be held together for study of that side of the scale that had been in contact with the alloy; the platinum was visible occasionally in the spectra but did not interfere. Scales were examined after the specimens had advanced well into the protective stage of oxidation. After analysis in the as-received condition, a compositional profile from the interface into the scale was obtained by successive bombardments by argon ions followed each time by analysis. Atomic concentrations were calculated by measuring the area under the most prominent photoelectron peak for each element, after a linear background subtraction, followed by use of the relative sensitivity factors of Wagner [12].

The atomic concentrations as a function of bombardment dose are plotted for each silicon bulk composition in Figures 9-12. The relationship between dose and depth is not well known for materials containing oxidised silicon, but it is likely that a dose of $1 \mu\text{A}\cdot\text{min}$ corresponds to removal of between 1 and 2 Å. As can be seen, the concentration of silicon near the metal/oxide interface increased progressively with bulk concentration. Figure 13 shows that the maximum atomic concentration found at the interface varies roughly linearly with the bulk concentration. However, the line does not go through the origin so that a truly linear relationship obviously does not hold. Although the atomic ratios of oxygen to silicon on the Fe^{1W}/O Si samples at depths where very little iron was present, are not 2:1, but much closer to 1:1, they should not be regarded as accurate on an absolute basis; a similar quantification carried out on a pure SiO₂ standard gave an O:Si ratio of 1.3:1. The formation of silica is therefore not precluded (although see below). At all the scale/metal interfaces examined a high level of carbon was also found, confirming the electron microprobe observation. Before bombardment some of the carbon would have arisen from pick-up from atmospheric or chemical contamination, but the erosion profiles show that carbon persisted to significant depths.

In addition to compositional information, XPS also provides chemical information based on photoelectron peak energies. For this work, standards of elemental silicon, of evaporated silicon monoxide,

of silicon dioxide as fused silica, and of synthetic Fayalite, Fe_2SiO_4 , were studied in an attempt to establish the nature of the silicon-rich layer at the interface. With the oxide standards, as opposed to the thin stripped scales on their platinum backing, there were problems of surface charging that made comparisons between the absolute energetic positions of individual photoelectron peaks impossible. However, charging shifts all peaks by the same amount so that comparisons based on peak energy separations are valid. The separation chosen for comparison here was that between the Si 2p and the O 1s peaks, since it turns out that the differences between them take on characteristic values for the standard materials. Table 5 lists these separations for the oxide standards, measured after ion bombardment, when the initial carbon contamination had been removed, and Table 6 lists the same parameter for the samples containing 0.4^w/o and 1.0^w/o Si, as a function of ion bombardment dose.

Clearly the presence of Fayalite is ruled out on the basis of this comparison; the difference between the Si-O peak separation in the synthetic Fayalite and in any of the scales at any stage of bombardment is well outside experimental error. Equally clearly the silicon-rich layer cannot be regarded as equivalent chemically to normal bulk silica. If the comparisons are appropriate, then the layer would appear to be oxygen-deficient with respect to SiO_2 , and this conclusion is supported by the result of the elemental quantification described above. On the other hand, Figure 7 reveals a fibrous structure in the layer, in which the silicon atoms may well have a co-ordination slightly different from that in bulk silica anyway.

Since the carbon 1s peak was always in the same energetic position, corresponding to uncombined carbon, and since the silicon peaks from the scales were always single, there was no reaction between the carbon from the oxidant CO_2 and the alloyed silicon. The large amount of carbon in the silicon-rich layer was thus present either as graphite or as amorphous carbon, consistent with the X-ray results described earlier. Although some of the carbon seen in the early stages of profiling contained a contribution from surface contamination, most of it must have come from the CO_2 .

2.6 Mössbauer Spectroscopy

A back reflection Mössbauer measurement, which had a depth penetration of around 1000 Å, was performed on the inner surface of the scale taken from an Fe 1^W/o Si alloy. The Mössbauer spectrum showed that the near surface region was composed largely of non-ferrous material.

3. DISCUSSION

The application of the phenomenological theory for the oxidation of binary iron-silicon alloys [13] suggests that for alloys containing less than 5 atom % of silicon an incomplete layer of silica should develop at the metal/scale interface and that as the interface proceeds into the metal, fragments of silicon-rich material must be left as precipitates in the inner scale. The interfacial film would decrease the oxidation rate of dilute iron-silicon alloys with respect to pure iron by partially blocking the transfer of iron atoms from the alloy into the scale. The location of the silicon in oxidized iron-silicon specimens described in this paper and shown schematically in Figure 14 largely supports these predictions.

The mechanism by which the silicon-containing species is being distributed between the inner layer and the rich layer adjacent to the metal seems to result in a steady state during the stage of protective oxidation considered in these experiments. The amounts of silicon in the inner scale and the thin layer do not appear to increase as oxidation proceeds and the silicon from the consumed alloy must be deposited in the inner scale as the metal/scale interface moves inwards.

A full understanding of the function of silicon in retarding the oxidation process is hampered by the lack of a completely accepted model for the oxidation of pure iron. The microstructural observations made here are of some help in this connection: the straight boundary between the inner and outer scales together with the abrupt changes in grain size and silicon content at the boundary are all consistent with the supposition that the boundary marks the original surface of the

metal coupon. It follows that the inner scale has grown by inward transport of oxidant, probably including the penetration of CO_2 to the base of the scale where carbon was found to accumulate. The outer scale has grown by outward migration of iron. The concurrent operation of these two mechanisms is consistent with the tracer measurements of Atkinson and Taylor [14]. The tracer measurements also indicate that the outward migration of cations occurs through oxide grain boundaries, as might be expected by analogy with nickel oxidation which proceeds via nickel oxide grain boundary transport at temperatures below 1000°C [15].

The silicon-containing material distributed through the inner part of the duplex scale represents a far lower concentration of silicon than that found in the very thin interfacial layer and it probably influences the oxidation rate to a much lesser extent. Indeed in view of the disparity in grain size (Figure 6b) and the importance of short circuit transport processes it is likely that the outer part of the duplex scale has more influence on the rate controlling processes than does the inner scale. For this reason changes in the oxidation kinetics are also more readily attributable to the silicon-rich layer at the scale/metal interface than to the silicon distributed generally in the inner scale. The apparent parabolic rate constant falls progressively as the silicon content of the alloy rises - to a critical value between 0.3 and 0.4W/o Si (Figure 15). In the region of this composition there appears to be a reduction in the slope of the function relating rate constant with silicon content.

Thermodynamic considerations [13] indicate that some of the silicon-rich layer ought to be Fayalite (Fe_2SiO_4) but the X-ray diffraction pattern of the underside of the scale shows only the same broad feature (at 3.4 \AA) that appeared on the electron diffraction patterns and the Mössbauer measurement fails to detect an iron-containing species. The evidence for the absence of Fayalite in the layer is completed by the XPS observations which show that there is indeed very little or no iron at the interface itself, and that neither the oxygen to silicon atomic ratios nor the silicon and oxygen energy separations are in agreement with those in Fayalite. On the other hand, XPS seems to suggest that the layer next to the alloy is

different chemically from bulk silica in being oxygen-deficient, both the elemental quantification and the energy separation data indicating a coordination state of silicon somewhere between those in silica and in silicon monoxide. Since the layer was seen to be fibrous by TEM, the comparison with bulk oxides may not be wholly valid, however.

In conclusion, we have observed that duplex scales on iron-silicon alloys oxidizing at reduced rates with respect to pure iron contain silicon at a low concentration throughout the inner part and at a high concentration in a very thin layer close to the metal/scale interface. The latter feature is thought to be mainly responsible for the reduced oxidation rate.

Acknowledgements

The authors are grateful to Miss L.S. Welch for electron microprobe measurements, to Dr. G. Longworth for the Mössbauer measurement, to Mr. J.S. Sears and to Mr. A. Nickerson for the oxidation experiments, to Dr. H.E. Bishop and Mr. N.R. Smart for XPS measurements, and to Messrs. T. Hughes and W. Young for specimen preparation. Helpful discussions with Dr. A.E. Hughes, Dr. A. Atkinson and Dr. A.M. Pritchard are also gratefully acknowledged.

References

- [1] A.M. Pritchard and A.E. Truswell, British Nuclear Energy Society Conference, Corrosion of steels in CO₂, Paper 19, 1974.
- [2] J.E. Antill, UK Patent 2,019,886, 1979.
- [3] I. Svedung and N.G. Vannerberg, Corros. Sci., 14, 391, 1974.
- [4] W.J. Tomlinson and J. Yates, Oxidation of Metals, 12, 323, 1978.
- [5] G.C. Wood, J.A. Richardson, M.G. Hobby and J. Boustead, Corros. Sci. (1969), 9, 659.
- [6] C. Tyzak and H.C. Cowen, Atomic Energy Review, 14, 263, 1976.
- [7] H.J. Yearian, W.D. Derbyshire and J.F. Radavich, Corrosion 13, 596, 1957.
- [8] N.N. Khoi, W.W. Smeltzer and J.D. Embury, J. Electrochem. Soc., 1975, 1495.
- [9] S.J. Bhatt and H.D. Merchant, J. Amer. Ceram. Soc. 52, 1969, 452.
- [10] A. Nakamura, S. Yamauchi, K. Feuki and T. Mukaibo, J. Phys. Chem. Solids 39, 1978, 1203.
- [11] R.J. Hussey, G.I. Sproule, D. Caplan and M.J. Graham, oxidation of Metals, 11, 1977, 65.
- [12] C.D. Wagner, Anal. Chem., 44, 1972, 1050.
- [13] A. Atkinson, 1980, AERE-R9960.
- [14] A. Atkinson and R.I. Taylor, 1980, unpublished results.
- [15] A. Atkinson and R.I. Taylor, 1980, Phil. Mag., in press.

Table 1

Silicon content of iron-silicon alloys, wt %

<u>Nominal</u>	<u>Actual</u>
0	<0.01
0.1	0.12 \pm 0.02
0.3	0.38 \pm 0.05
0.7	1.04 \pm 0.09

Table 2

Texture Coefficient $T_{h'k'l}$ of Alloys and Scales

Substrate α Fe

<u>Composition</u>	T_{h00}
Fe	2.4
Fe 0.1 ^W /o Si	0.6
Fe 0.4 ^W /o Si	1.1
Fe 1 ^W /o Si	0.7

Scale formed in CO₂ 900 vpm air - α Fe₂O₃

<u>Composition</u>	T_{h00}
Fe	6.9
Fe 0.1 ^W /o Si	6.8
Fe 0.4 ^W /o Si	6.0
Fe 1 ^W /o Si	6.5

Scale formed in CO₂ 1% CO - Fe₃O₄

<u>Composition</u>	T_{h00}
Fe	3.7
Fe 0.1 ^W /o Si	2.2
Fe 0.4 ^W /o Si	1.6
Fe 1 ^W /o Si	3.0

*Texture coefficients $T_{h'k'l}$ for a purely randomly oriented material would be 1.00. For calculation purposes the intensities used for randomly oriented materials were those given by the Joint Committee on Powder Diffraction Standards records.

Table 3

Mean kinetic constants (and standard deviation) for iron and iron-silicon alloys oxidized in CO₂ 1% CO at 500°C

<u>Composition</u>	<u>Parabolic Rate Constant</u>	<u>Value of n in</u>
	$\frac{\text{gm}^2}{\text{cm}^4 \text{Sec}} \times 10^{12}$	<u>equation $\Delta w = kt^n$</u>
Fe	7.97 (0.36)	0.414 (0.012)
Fe 0.1 ^w /o Si	6.60 (0.32)	0.408 (0.030)
Fe 0.4 ^w /o Si	2.33 (0.14)	0.348 (0.022)
Fe 1 ^w /o Si	1.04 (0.06)	0.262 (0.013)

Table 4

Wavelength dispersive X-ray analysis of polished sections through scales on 5 specimens

Specimen Composition (a)	Weight Gain mg cm ⁻²	Site of Analysis	Composition %			
			Si (b)	Fe	O	Total
Fe	3.7	outer scale	0.0	73.3	28.6	101.9
		inner scale	0.0	71.9	26.6	98.5
Fe 0.1% Si	3.1	outer scale	0.0	69.4	28.5	97.9
		inner scale	0.2	68.0	24.9	93.2
		metal	0.1	100.7	0.0	100.8
Fe 0.4% Si	2.8	outer scale	0.0	71.7	28.9	100.5
		inner scale	0.4	72.7	30.5	103.6
		metal	0.2	98.4	0.0	98.7
Fe 1% Si	3.9	outer scale	0.0	72.7	30.9	103.5
		inner scale	1.6	70.9	30.3	102.8
		metal	0.9	99.2	0.0	100.1
Fe 1% Si	2.9	outer scale	0.0	68.2	22.4	90.6
		inner scale	1.8	67.0	23.6	92.5
		metal	1.1	92.9	0.1	94.0

(a) 1% Si in Fe corresponds to 3.2 %.

(b) 1% Si in Fe₃O₄ corresponds to 2.2%.

Carbon levels were not significantly above the background level on these specimens.

Nominal compositions of Fe₃O₄ is Fe 72.4, O 27.6%.

Table 5

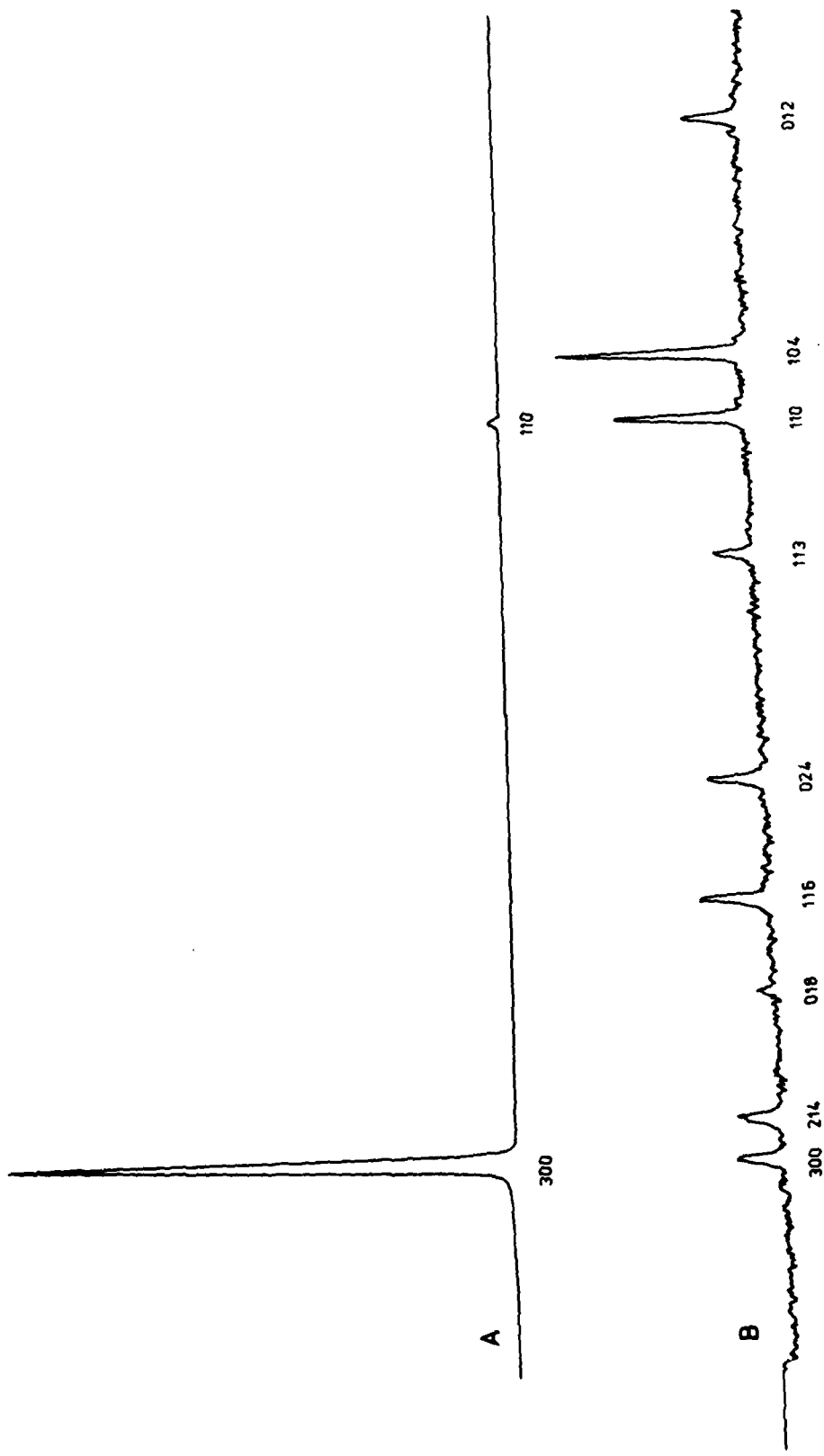
The energy separation (in eV) of the Si 2p and O1s peaks for oxygen-containing silicon compound standards after 50 μ A min ion bombardment at 5 keV.

Evaporated SiO	Fused Silica SiO ₂	Synthetic Fayalite Fe ₂ SiO ₄
429.8	429.2	428.0

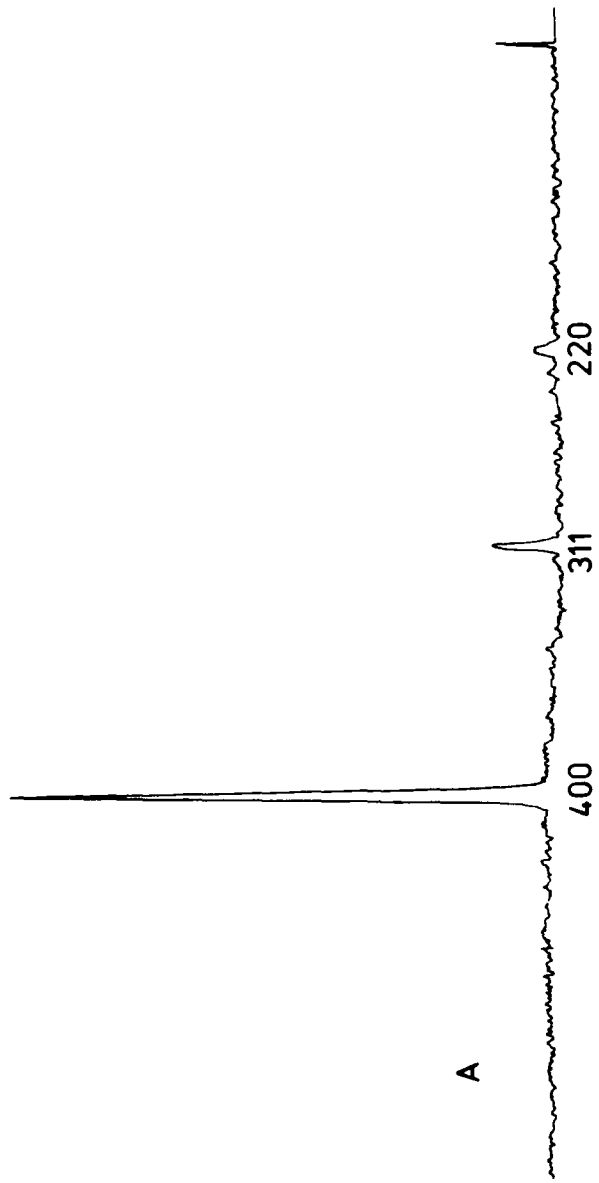
Table 6

The energy separation (in eV) of the Si 2p and O1s peaks for scales on the alloys Fe/0.4% Si and Fe/1.0% Si as a function of ion bombardment dose (experimental error \pm 0.1 eV.)

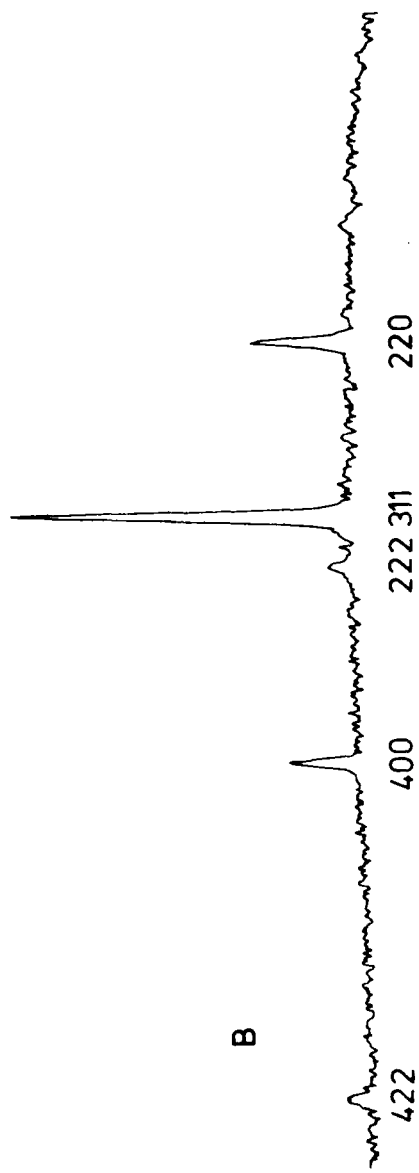
Fe/0.4 % Si				Fe/1.0 % Si			
Sample A		Sample B		Sample A		Sample B	
IB μ A min	eV	IB μ A min	eV	IB μ A min	eV	IB μ A min	Ev
0	428.8	0	429.6	0	430.2	0	429.8
10	429.4	10	429.8	15	430.4	10	429.8
40	429.6	50	429.2	50	430.2	60	429.6
140	429.4	190	430.0	150	429.8	160	430.4
440	429.4	390	429.6	350	430.0	460	429.6



AERE - R 10042 Fig. 1
 X-ray powder diffraction patterns. A. Outer surface of scale grown on α iron in $\text{CO}_2/900$ vpm air.
 B. Standard random pattern of $\alpha\text{Fe}_2\text{O}_3$.

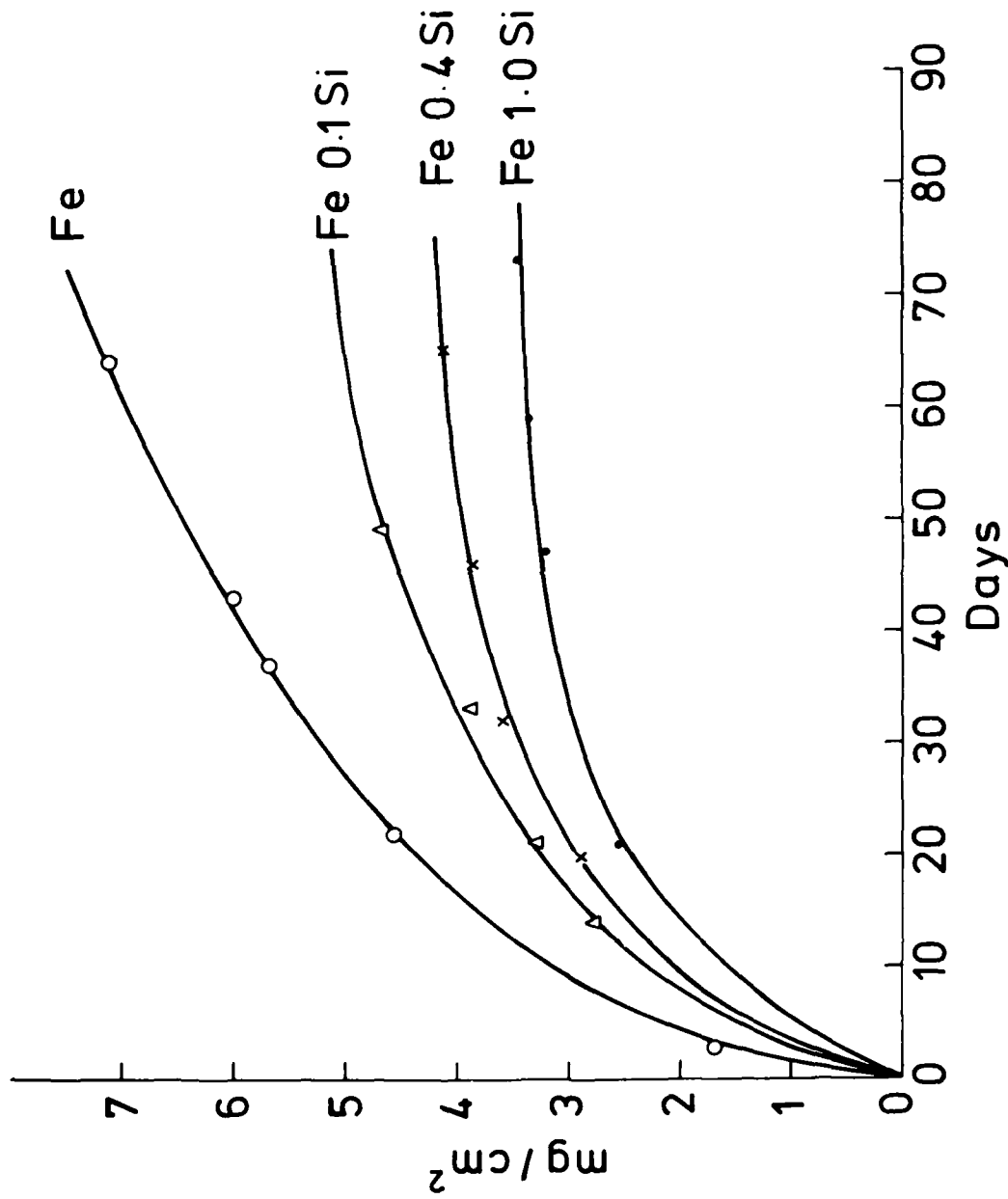


A

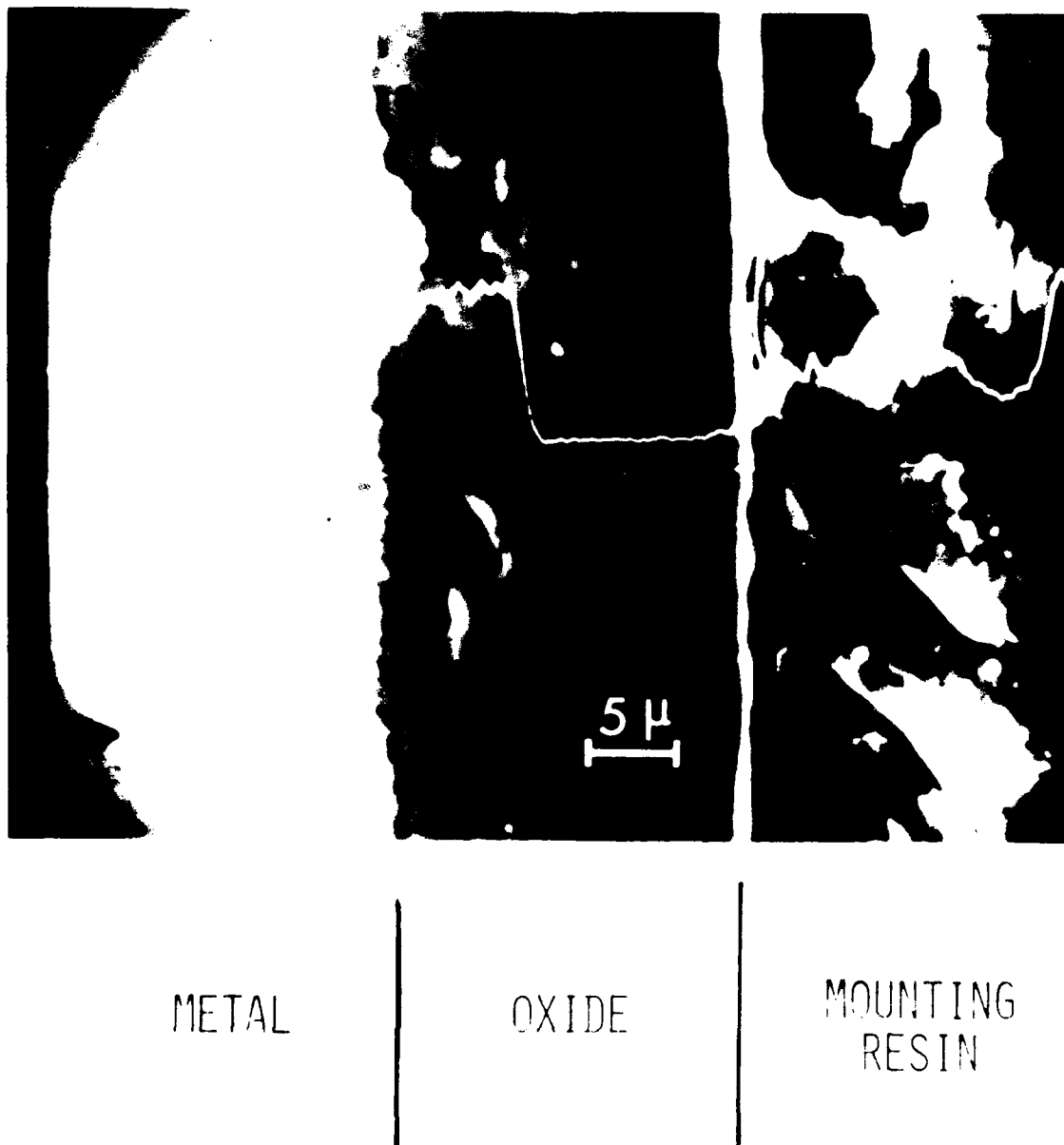


B

AERE - R 10042 Fig. 2
 X-ray powder diffraction patterns. A. Outer surface of scale grown on α iron in CO_2 /1% CO.
 B. Standard random pattern of Fe_3O_4 .

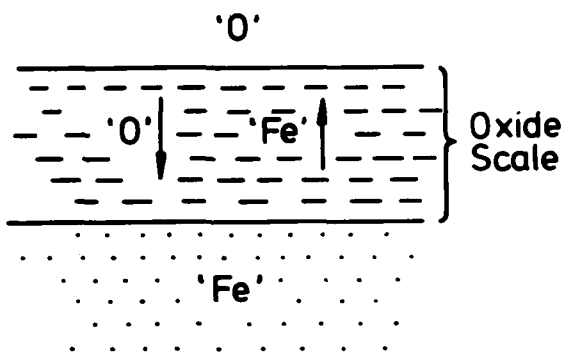


AERE - R 10042 Fig. 3
 Weight gain curves of pure iron and iron silicon alloys oxidized in $\text{CO}_2/1\% \text{CO}$ at 500°C .

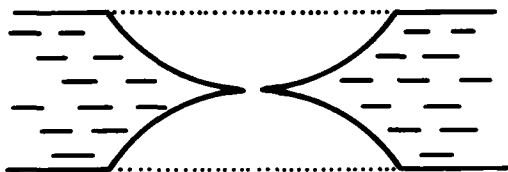


AERE - R 10042 Fig. 4

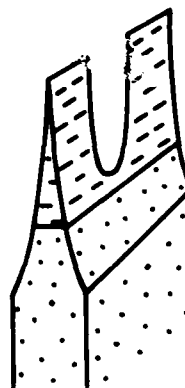
Scanning electron micrograph of section through metal and scale on Fe 1 W 0 Si. The trace is a scan for silicon made along the indicated line. Note that the zero of silicon signal is not on this line but corresponds to the value in the outer part of the scale.



(a)



(b)



(c)

AERE - R 10042 Fig. 5

(a) Development of oxide scale on a metal surface and preparation of (b) parallel and (c) transverse specimens for electron microscopy.

SCALE/GAS
INTERFACE



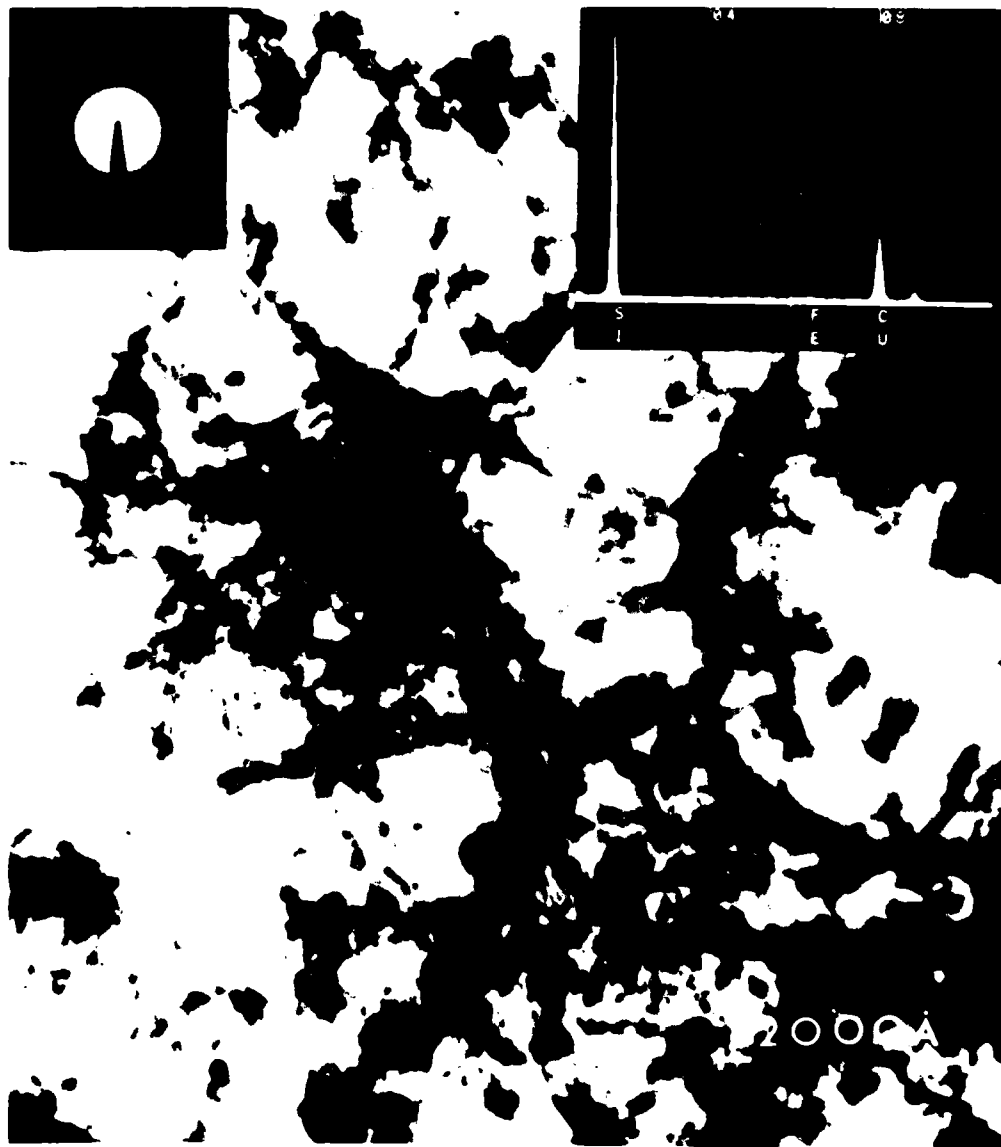
AERE - R 10042 Fig. 6(a)
Transverse transmission electron micrographs of scale grown on a specimen of Fe 0.1 w/o Si.
Outer scale.



AERE - R 10042 Fig. 6(b)
Transverse transmission electron micrographs of scale grown on a specimen of Fe 0.1 W 0 Si.
Boundary between outer and inner scale (arrowed).



AERE - R 10042 Fig. 6(c)
Transverse transmission electron micrographs of scale grown on a specimen of Fe 0.1 W/o Si.
Boundary between inner scale and metal.



AERE - R 10042 Fig. 7

Plan transmission electron micrograph of material taken from between the metal and the oxide scale after oxidation of an Fe 1 W/o Si alloy in CO₂/1% CO at 500°C for 3 months. Insets show an EDAX spectrum and a diffraction pattern from this material.



Scanning electron micrograph



Oxygen map



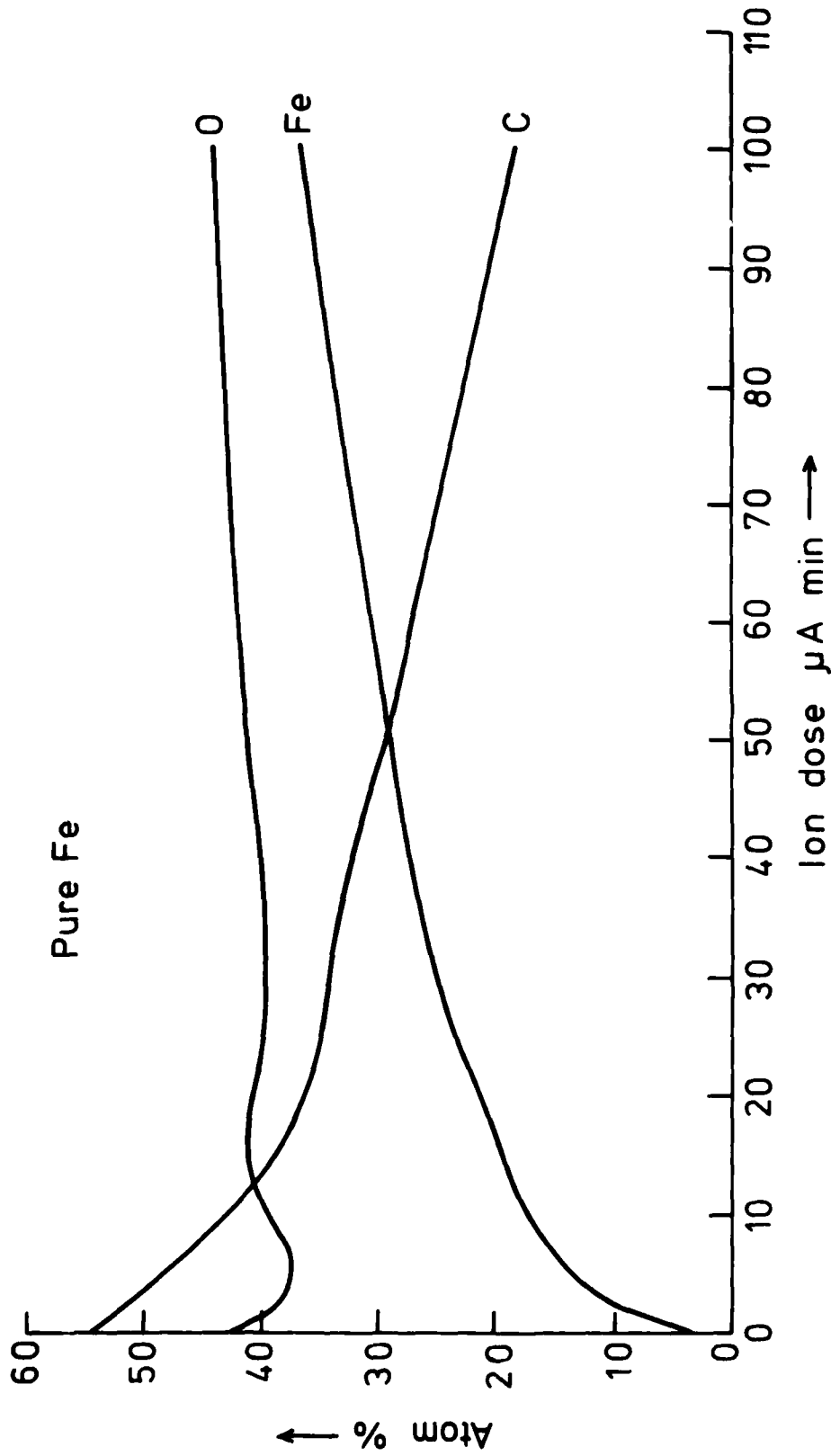
Silicon map



Carbon map

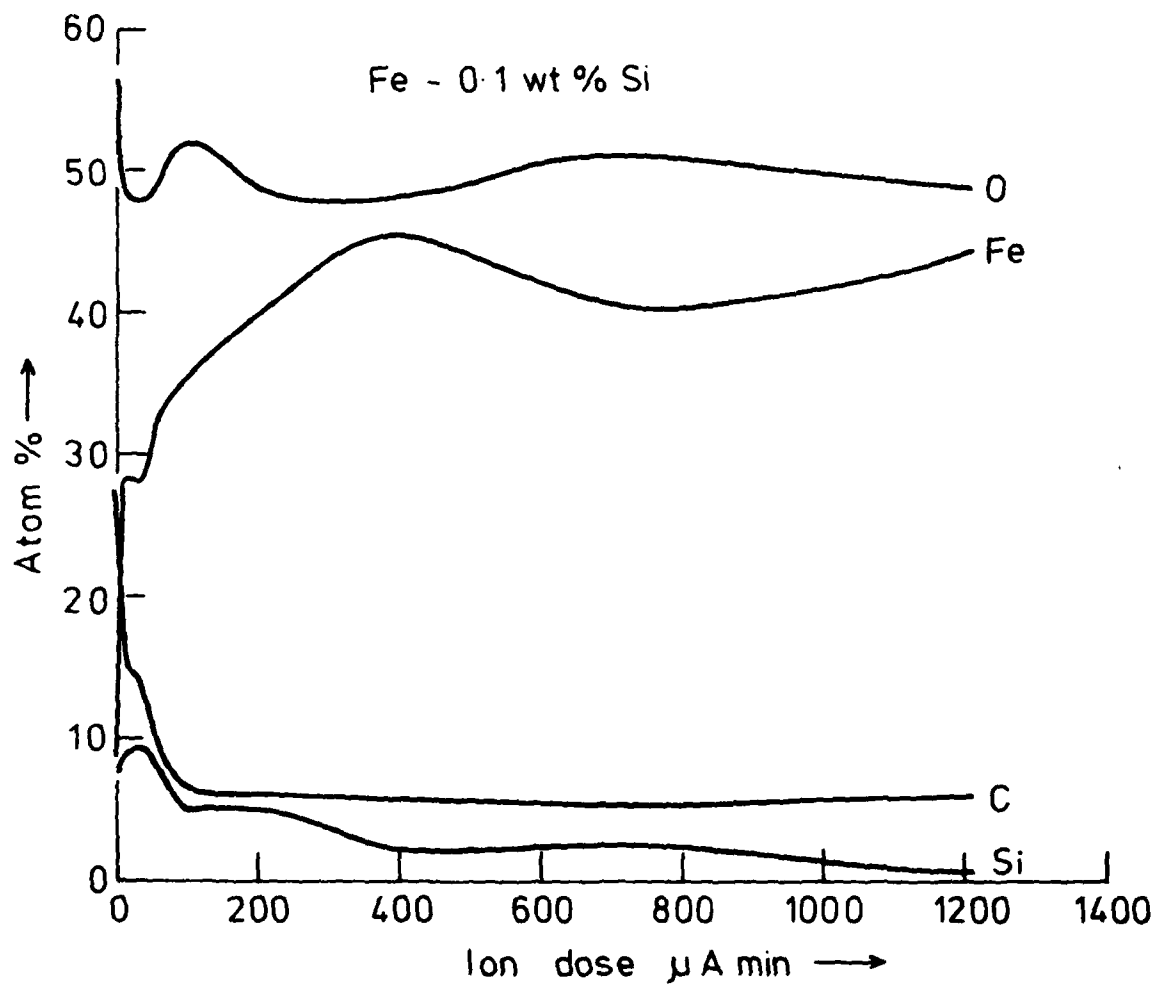
Interfacial layer from between the Fe 1^W/o Si alloy and its protective oxide

AERE - R 10042 Fig. 8
SEM image (a) together with oxygen (b), silicon (c) and carbon (d) maps (all x 800) of material from
between Fe 1^W/o Si and scale.



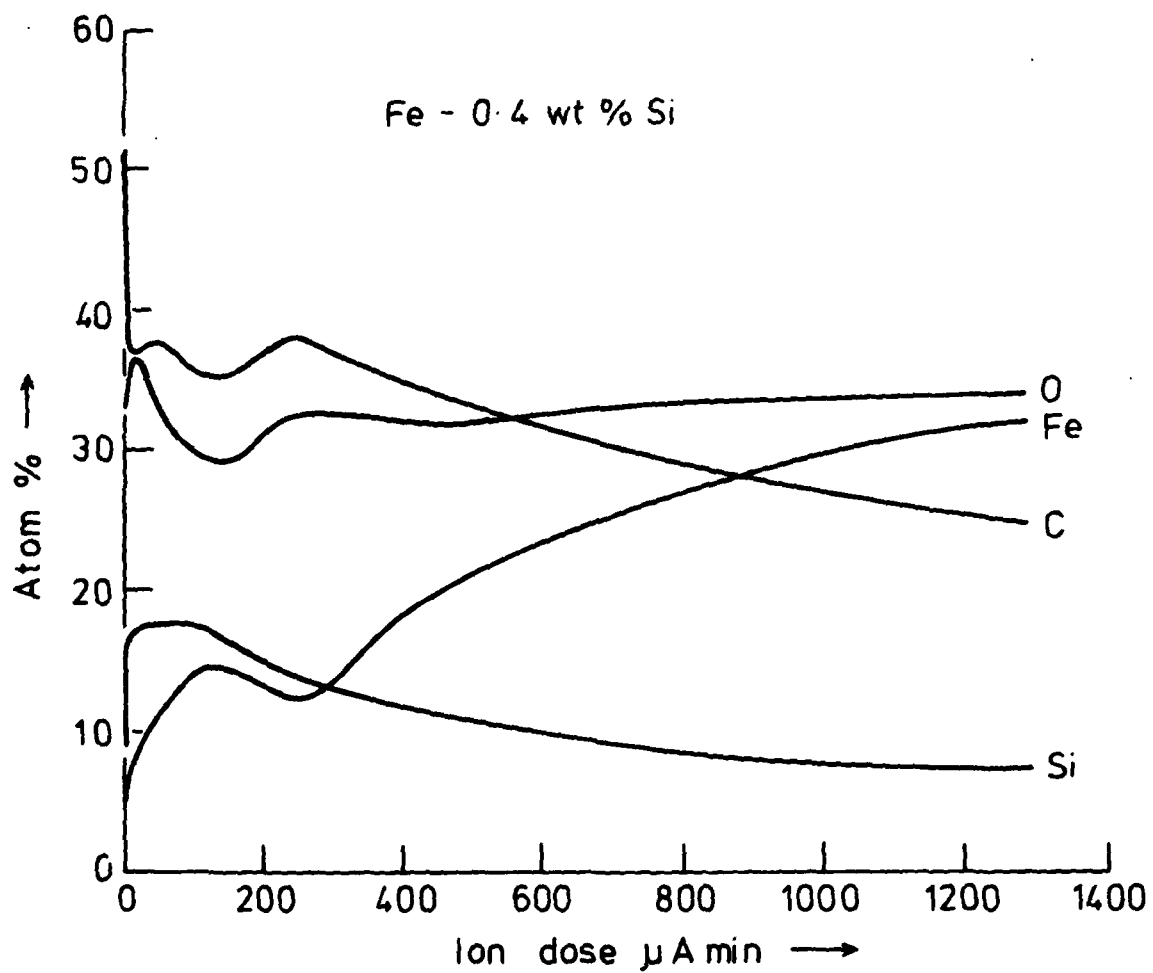
AERE - R 10042 Fig. 9

Depth profile of elemental composition measured by XPS. The initial surface at zero ion dose was that of the underside of the scale grown on pure Fe. Erosion by an ion beam coupled with XPS analysis then gave the composition as a function of distance into the oxide.



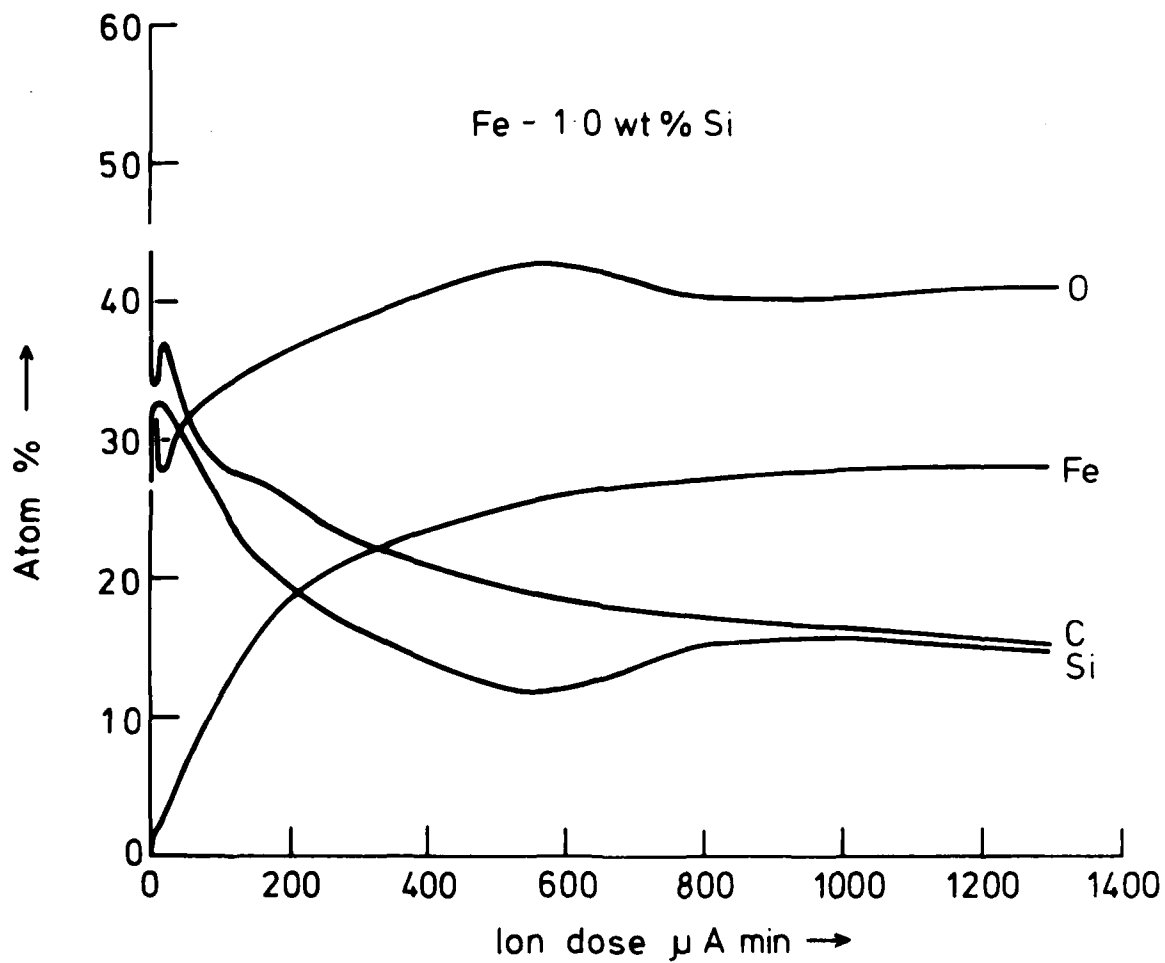
AERE - R 10042 Fig. 10

Depth profile of elemental composition measured by XPS. The initial surface at zero ion dose was that of the underside of the scale grown on the Fe/0.1 W/o Si alloy. Erosion by an ion beam coupled with XPS analysis then gave the composition as a function of distance into the oxide.



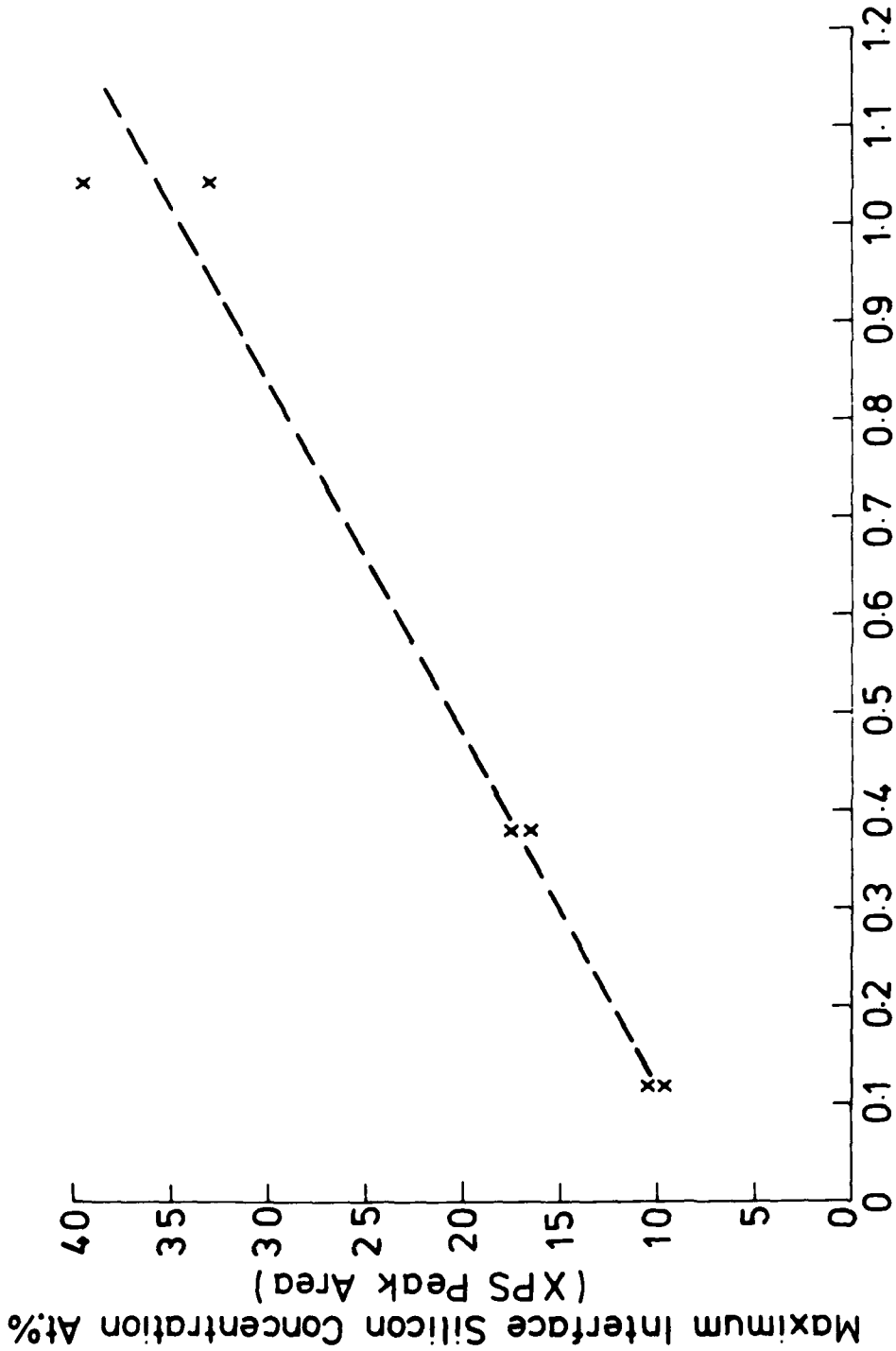
AERE - R 10042 Fig. 11

Depth profile of elemental composition measured by XPS. The initial surface at zero ion dose was that of the underside of the scale grown on the Fe/0.4 wt% Si alloy. Erosion by an ion beam coupled with XPS analysis then gave the composition as a function of distance into the oxide.



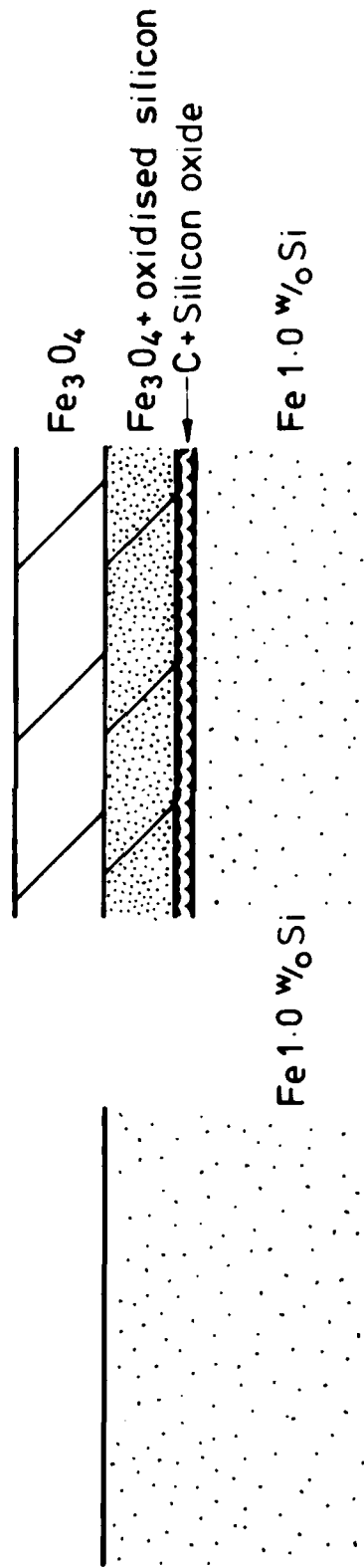
AERE - R 10042 Fig. 12

Depth profile of elemental composition measured by XPS. The initial surface of zero ion dose was that of the underside of the scale grown on the Fe/1 wt% Si alloy. Erosion by an ion beam coupled with XPS analysis then gave the composition as a function of distance into the oxide.

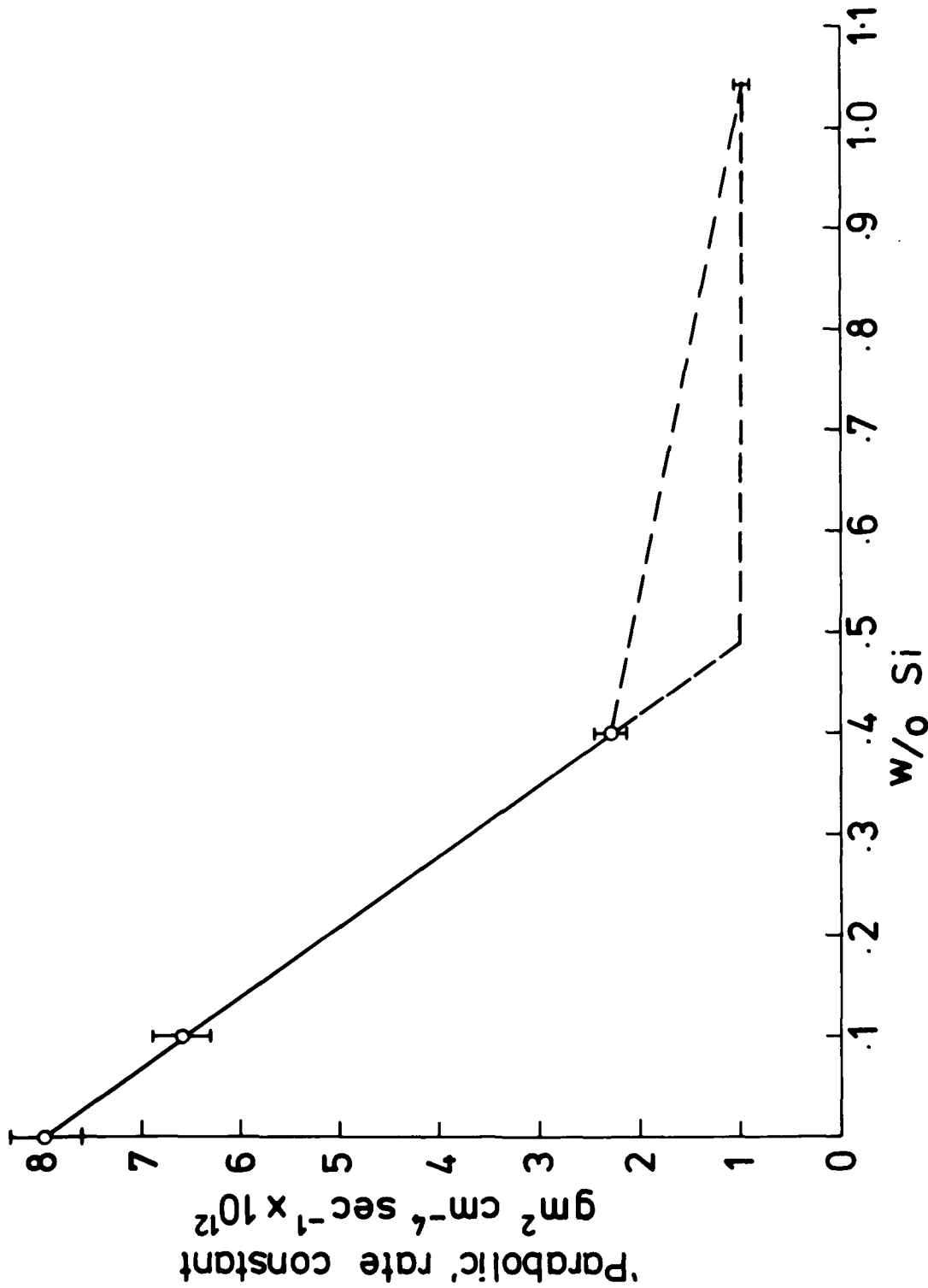


AERE - R 10042 Fig. 13

Variation of maximum peak silicon concentration in the interfacial layer as a function of silicon concentration in the alloy.



AERE - R 10042 Fig. 14
 Schematic drawing of near-surface region of Fe/Si alloy before and after protective oxidation with qualitative indication of silicon distribution.



AERE - R 10042 Fig. 15
 Variation of apparent parabolic rate constant for oxidation of Fe/Si alloys plotted as a function of silicon content.

**DA
FIL**